THE JOURNAL OF PHYSICAL CHEMISTRY B

Article

pubs.acs.org/JPCB

# Factors That Drive Peptide Assembly and Fibril Formation: Experimental and Theoretical Analysis of Sup35 NNQQNY Mutants

Thanh D. Do,[†] Nicholas J. Economou,[†] Nichole E. LaPointe,[‡] William M. Kincannon,[†] Christian Bleiholder,[†] Stuart C. Feinstein,[‡] David B. Teplow,[§] Steven K. Buratto,[†] and Michael T. Bowers*[,†]

[†]Department of Chemistry and Biochemistry and [‡]Neuroscience Research Institute and Department of Molecular, Cellular and Developmental Biology, University of California, Santa Barbara, California 93106, United States

[§]Department of Neurology, David Geffen School of Medicine at UCLA, Mary S. Easton Center for Alzheimer's Disease Research at UCLA, and Brain Research Institute and Molecular Biology Institute, University of California, Los Angeles, California 90095, United States

Supporting Information

**ABSTRACT:** Residue mutations have substantial effects on aggregation kinetics and propensities of amyloid peptides and their aggregate morphologies. Such effects are attributed to conformational transitions accessed by various types of oligomers such as steric zipper or single $\beta$-sheet. We have studied the aggregation propensities of six NNQQNY mutants: NVVVVY, NNVVNV, NNVVNY, VIQVVY, NVVQIY, and NVQVVY in water using a combination of ion-mobility mass spectrometry, transmission electron microscopy, atomic force microscopy, and all-atom molecular dynamics simulations. Our data show a strong correlation between the tendency to form early $\beta$-sheet oligomers and the subsequent aggregation propensity. Our molecular dynamics simulations indicate that the stability of a steric zipper structure can enhance the propensity for fibril formation. Such stability can be attained by either hydrophobic interactions in the mutant peptide or polar side-chain interdigitations in the wild-type peptide. The overall results display only modest agreement with the aggregation propensity prediction methods such as PASTA, Zyggregator, and RosettaProfile, suggesting the need for better parametrization and model peptides for these algorithms.

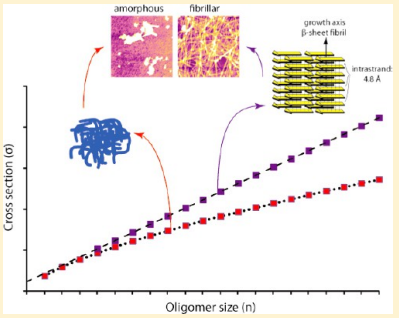


## INTRODUCTION

The nature of biomolecular self-assembly, including its driving forces, mechanisms, kinetics, and biological functions, has been a topic of active research in recent decades.[1−3] Advanced techniques have been used to unravel the interactions and dynamics of aggregation from the atomic to the macroscopic level. In the quest to understand disease-related aggregation processes,[2,4−6] several general mechanisms describing the aggregation of biological systems have been proposed with a common feature of fibril formation arising from a conformational transition or series of transitions during the assembly process.[7−9] The most challenging aspect of this puzzle is that peptides with similar primary structures (wild-type versus mutants/variants) can behave very differently, whereas those with distinct sequences may show similar properties. For example, the simplest single-point mutation can dramatically suppress or accelerate the aggregation process of amyloid peptides.[10] Consequently, it is a difficult task for any statistical model dependent on sequence homology to predict aggregation propensity.[11] A more categorical approach has been established emphasizing the nonlocalized properties of the peptides, namely, amino acid composition,[12] peptide length,[13] and the ability to form certain nucleation units such as a $\beta$-sheet or steric zipper, to circumvent this issue.[14,15]

The steric zipper, first shown experimentally by X-ray crystallographic data of (G)NNQQNY,[16,17] has been hypothesized to not only serve as the spine of the protofilament, but also to facilitate interactions among larger protofilaments-subunits.[18] The steric zipper is composed of two $\beta$-sheet layers with intra- and intersheet spacings of ∼0.5 nm and 1.0 to 1.5 nm, respectively.[17] Because of this structure's central role in amyloid polymorphism, the steric zipper has been viewed as a reliable indicator to distinguish fibril formation from other self-assembly motifs such as amorphous or annular aggregates.[19] The nature of the zipper structure satisfies the definition of fibril character, specifically high $\beta$-sheet content stabilized by a hydrogen-bond network within each layer, and minimized exposure of hydrophobic surfaces by hydrophobic or polar interactions. The bilayer motif affords aggregation growth to a size (∼10 nm in width) consistent with observations by microscopy.[20,21] Many fibril structures solved by X-ray crystallography contain the zipper motifs,[14,22,23] suggesting that fibrils exist as an extension of this polymorphism. However, the contribution of the steric zipper to aggregation propensity

**Received:** May 9, 2013
**Revised:** June 24, 2013
**Published:** June 26, 2013

ACS Publications © 2013 American Chemical Society

(especially kinetics) remains unclear. Is a peptide that forms steric zipper oligomers also a fibril-forming peptide? Can a scoring scheme be developed to quantify the aggregation propensity of a peptide based on its tendency to form a steric zipper?

Answers to these questions have been proposed using NNQQNY as a template to construct steric zipper motifs for random sequences and to assign scores relative to the known aggregation propensity of (G)NNQQNY. The early success of this approach, known as the RosettaProfile method,[24,25] in predicting aggregation-prone fragments suggests that it may be a promising protocol for the design of self-assembled biomolecules.[25] It is important to note that steric zippers have been predicted computationally for fragments of various proteins at the level of oligomer, including tau (hexapeptides PHF6 [VQIVYK] and PHF6* [VQIINK]),[26,27] islet amyloid polypeptide (SSTNVG),[28] amyloid $\beta$-protein (KLVFFAE),[29] insulin (VEALYL),[27,30] and $\alpha$-synuclein (GVATVA).[30] Experimental evidence has been consistent with the theoretical models of some peptides.[9,26,31,32] However, there exist peptide sequences (e.g., NNFGAIL)[14,33] for which X-ray crystallography is inconsistent with a central role for a steric zipper, in that the data show little to no interdigitation between $\beta$-sheets although the overall bilayer is retained.

The steric zipper conformation can be energetically favored,[29] but the formation of such a motif in the early stages of aggregation may not be sufficient for subsequent fibril formation. Here we use a combination of experimental and computational techniques to examine the contribution of the steric zipper motif to a peptide's aggregation propensity. Starting with the yeast prion Sup35 fragment NNQQNY, we performed mutations to obtain a series of peptides with increased hydrophobic character. It has been suggested that the steric zipper polymorphism is favored by the unique properties of Asn and Gln residues.[34] Our mutations that replace bulky and polar Asn and Gln residues with smaller or more hydrophobic residues (Val and Ile) may suppress the stability of the steric zipper motif by disrupting the selective side chain interactions within the dry interface.[35] Our study utilizes ion-mobility mass spectrometry (IM-MS), transmission electron microscopy (TEM), atomic force microscopy (AFM), and explicit solvent molecular dynamics (MD) simulations to elucidate correlations between early oligomer conformations and macroscopic aggregate morphologies. This combination of complementary techniques provides a detailed picture of the aggregation process, especially the contribution of early oligomer structures to aggregation kinetics and propensities.

## MATERIALS, METHODS, AND MUTANTS

**Mutants of Yeast Prion Sup35 NNQQNY.** A set of 2 500 000 different random mutations of the peptide NNQQNY were generated. These mutants include single, double, triple, and quadruple mutants. Subsequently, the Prediction of Amyloid STructure Aggregation (PASTA) score was computed for each peptide sequence. A PASTA score of less than −4 indicates a very strong $\beta$-aggregation propensity.[36,37] From this set of sequences, six were selected for further study based on a strongly negative PASTA score (NNQQNY is +1.65) and on similarity to the original sequence NNQQNY (measured by number of identical residues). An additional aggregation scoring method, Zyggregator,[38,39] was used to further characterize the six mutants. In Zyggregator, the more positive the score, the more likely the peptide is to aggregate. Each mutant was also analyzed by the RosettaProfile method to obtain a composite score (C-score),[24,25] evaluating aggregation propensity based on the steric zipper NNQQNY model. (See Figure S1 in the Supporting Information.) The C-score takes into account the energy of one layer composed of two $\beta$-strands (2 × 6 residues), area of interface, shape complementary, and solvent accessible area. The six mutants used in this project have similar C-scores to NNQQNY and are well below Rosetta's energy threshold of −23 kcal/mol. The structures for the seven peptides are given in Figure 1, and the rankings of the series for each method are shown in Table 1.

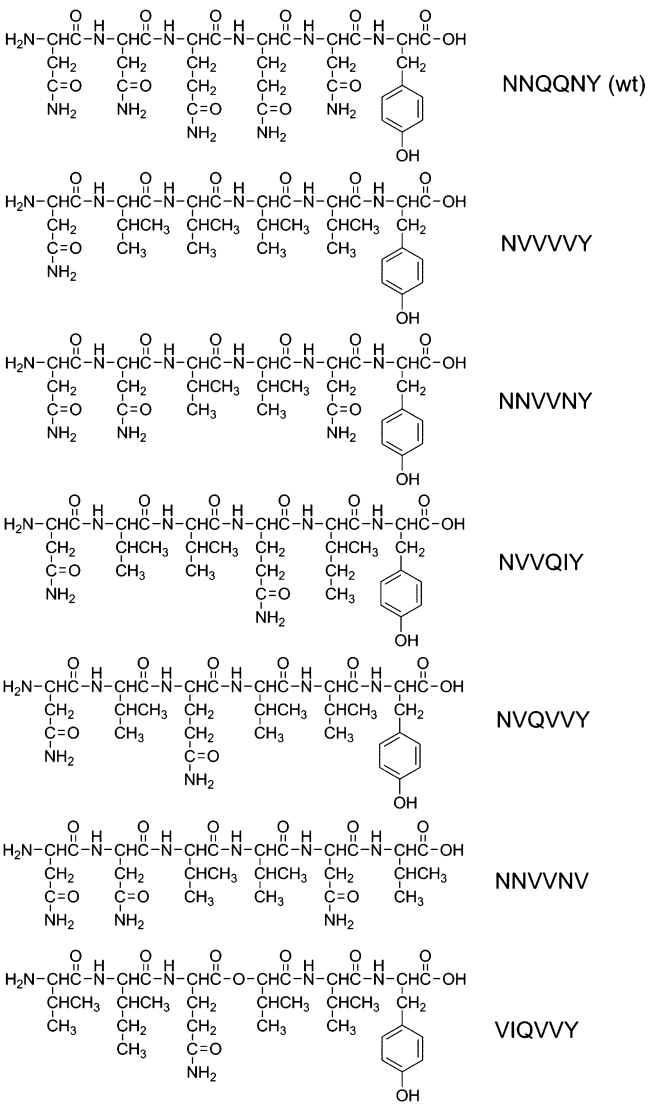


**Figure 1.** Chemical structures of NNQQNY and the six mutants.

The mutant selection methods indicate the importance of the Gln residues for steric zipper formation, as two out of three mutants lacking of this motif (NNVVNV and NNVVNY) are ranked lower than the wt NNQQNY by RosettaProfile. (Note that this method evaluates aggregation propensity based on steric zipper formation.) The difference in aggregation propensity of these two mutants allows comparison of valine to tyrosine in position 6. All methods except Zyggregator favor Val over Tyr, which, at first glance, is counterintuitive because Tyr can contribute to oligomer stability through $\pi$-stacking. All


dx.doi.org/10.1021/jp4046287 | J. Phys. Chem. B 2013, 117, 8436−8446

**Table 1. Aggregation Propensity Scores for NNQQNY and Its Mutants Were Obtained from the PASTA, Zyggregator, and RosettaProfile Methods[a]**

| peptides | PASTA | Zyggregator | RosettaProfile |
|---|---|---|---|
| NNQQNY | 1.65 (7) | 0.36 (7) | −42.9 (5) |
| NVVVVY | −8.45 (1) | 1.70 (1) | −44.1 (3) |
| NNVVNV | −6.54 (3) | 1.18 (6) | −41.5 (6) |
| NNVVNY | −4.68 (6) | 1.21 (5) | −41.0 (7) |
| VIQVVY | −7.12 (2) | 1.43 (2) | −46.9 (1) |
| NVVQIY | −5.23 (5) | 1.24 (4) | −45.3 (2) |
| NVQVVY | −5.29 (4) | 1.28 (3) | −43.0 (4) |

[a]Number inside the parentheses is the rank for each peptide based on predicted aggregation propensity, from the highest to the lowest.

methods except PASTA ordered these two peptides at the bottom of the list.

The remaining four mutants (VIQVVY, NVVQIY, NVQVVY, and NVVVVY) are predicted to have medium to very high aggregation propensities. In the steric zipper model, Asn-X-Gln-X-Asn in (G)NNQQNY is the central core associating the two neighboring sheets.[17] If side-chain interdigitations in the steric zipper formation control the kinetics of aggregation, then mutation to less bulky or more hydrophobic residues should decrease aggregation propensity by decreasing steric zipper formation.[35] However, the ranking provided by RosettaProfile favors VIQVVY, NVVQIY, and NVVVVY over the wt. Additionally, by RosettaProfile, the more hydrophobic mutants have a higher predicted aggregation propensity. In VIQVVY, all residues except Gln-3 and Tyr-6 are replaced by hydrophobic residues. Interestingly, this mutant is consistently ranked first or second in the list by all methods. The mutant with an all hydrophobic core and almost all bulky residues (Asn and Gln) mutated to valine (i.e., NVVVVY) also appears very high in the list. Similarly, only Asn-1, Gln-4, and Tyr-6 remain intact in the mutant NVVQIY, but the peptide is also on the top of the list (below VIQVVY). The last sequence, NVQVVY, in which only Asn-5 is missing from the original core (Asn-X-Gln-X-Asn), is predicted to have a relatively modest aggregation propensity compared with the other mutants.

**Sample Preparation.** The NNQQNY peptide was purchased from Genscript (Piscataway, NJ) with $NH_2$ and COOH free termini. All other peptides were synthesized by FMOC (*N*-(9-fluorenyl)methoxycarbonyl) chemistry with free termini. The peptides were purified by reverse-phase HPLC and characterized by mass spectrometry and amino acid analysis. Stock solutions were prepared at the concentration of 2.0 mg/mL in hexafluoroisopropanol (TCI America) to disrupt oligomer formation and prevent aggregation. Aliquots of stock solutions were evaporated overnight before dilution in micrometer-filtered HPLC water to a final concentration of 400 $\mu$M. The choice of solvent is consistent with previous work done by our group[9] and others.[40,41]

**Instrumentation.** *Ion-Mobility Mass Spectrometry (IM-MS).* IM-MS is a versatile technique capable of characterizing oligomers without external modification to the systems.[9,42,43] The IM-MS instrument is built in-house and consists of a nanoelectrospray source, an ion funnel, a 200 cm long drift cell and a quadrupole mass filter.[44] A long drift cell offers high resolution in ion mobility experiments, where oligomers and conformations of the same $m/z$ species can be resolved with cross section difference of 1%.

In IM-MS, ions are formed from solution by ESI, captured by an ion funnel and then pulsed into a drift cell filled with helium gas. Upon exiting the drift cell, the ion species of interest are selected by a mass analyzer and passed on to the detector. From this process, an arrival-time distribution (ATD) of the analyte can be obtained. The presence of multiple features in the ATD for a specific mass-to-charge ratio ($m/z$) indicates either multiple conformers at that $m/z$, or multiple oligomers with the same reduced $n/z$ ($n$ = oligomer number, $z$ = charge). The arrival time of an ion at the detector, $t_A$, can be measured at different pressure to drift voltage ratios ($P/V$) to obtain the reduced mobility $K_0$ and collision cross section $\sigma$.[45,46]

Areas under the curve of various features in an ATD give the relative abundance of each species present. The shape of an ATD peak for a given species can be predicted using the kinetic theory of gases. If a measured ATD peak is broader than expected and cannot be separated into multiple features due to insufficient instrument resolution, then we can fit the broad distribution with multiple theoretical peaks using their heights and exact arrival times as variables.[47] More details of this process can be found in the Supporting Information (SI).

*Transmission Electron Microscopy.* Prior to obtaining TEM data, 400 $\mu$M samples were incubated at room temperature for 1 to 6 weeks and were checked with mass spectrometry to ensure no degradation had occurred. To prepare samples for TEM, peptides were fixed in 1.6% glutaraldehyde (Electron Microscopy Sciences) for 15 min at room temperature. A drop of the fixed sample was then placed on a 300-mesh Formvar/carbon-coated copper grid (Electron Microscopy Sciences) and allowed to absorb for 1.5 min. After this time, excess sample was wicked away, and the grid was coated with 1 mg/mL cytochrome c for 15 s (to encourage even staining), rinsed with deionized water to remove the cytochrome c, and then negatively stained with 2% uranyl acetate (Ted Pella) for 20 s. Grids were viewed on a JEOL-1230 TEM microscope at 80 kV. Digital images were acquired using an ORCA camera and AMT Image Capture Software (version 5.24).

*Atomic Force Microscopy.* AFM data were collected for 400 $\mu$M samples at similar incubation times as those for TEM. AFM images were collected using an Asylum MFP-3D-SA system (Asylum Research, Santa Barbara, CA). A silicon cantilever (MikroMasch NSC-15) with nominal resonant frequency of 325 kHz and spring constant of 40 N/m was employed in tapping mode. The cantilever was tuned to the resonant frequency at a voltage of 1 V, corresponding to a ∼50 nm free amplitude. An amplitude set point ratio ($R/R_0$) of 75−80% was used to achieve optimal height tracking as well as to keep the tip stably in attractive mode (phase >90°). All images were collected at 1 Hz using 512 × 512 scan points. Images were processed using Igor Pro software and were modified by masking fibrils and then applying a first-order flatten to the height and phase images ("Magic Mask" in MFP3D software). No further image modification was used.

**Molecular Dynamics Simulations.** Initial conformations for the steric zipper decamers were obtained from the RosettaProfile method.[25] Each steric zipper consisted of two $\beta$-sheet layers with five peptide chains per layer. The initial conformations were solvated in a 70 Å cubic water box and then minimized using steepest descent method. The number of water molecules in each system was 11 000. Simulations were performed using the GROMACS 4.5.5 package[48,49] and the all-atom optimized potentials for liquid simulations (OPLS-AA) force field[50−52] in TIP3P water[53] with periodic boundary


dx.doi.org/10.1021/jp4046287 | J. Phys. Chem. B 2013, 117, 8436−8446

condition. The LINCS algorithm[54] was employed to constrain bonds between heavy atoms and hydrogen, and the SETTLE algorithm[55] was used for water molecules. These constraints allowed an integration time step of 2.0 fs. The electrostatic and dispersion forces were computed with a real space cutoff of 1.2 nm, and particle mesh Ewald method[56,57] was used to treat long-range electrostatics. Temperature was maintained by the Nosé–Hoover thermostat.[58] The temperature and pressure coupling constants were 0.1 and 1.0 ps, respectively. Equations of motion were integrated according to the leapfrog algorithm. Solvent and volume equilibration was performed in NPT ensemble ($T$ = 300 K and $P$ = 1 bar). Production run was performed in NVT ensemble for 100 ns. The root-mean-square deviation (RMSD) is calculated using the initial conformation as reference. Center-of-mass distances between $\beta$-sheet layers for each snapshot were computed based on the average distances between the two planes spanned by the backbone atoms of each layer.

## RESULTS AND DISCUSSION

**NNQQNY Aggregates Weakly with a Long Lag Phase.** As previously mentioned, fragments containing the NNQQ pattern, especially NNQQNY and GNNQQNY, have been one of the benchmark models for fibrillar self-assembly.[25] It is widely held that the contribution of the terminal glycine to aggregation is negligible. As a result, NNQQNY is predicted to inherit the properties of the longer fragment GNNQQNY. Despite a tremendous amount of theoretical work done on these systems,[29,34,35,59−64] available microscopy data are very limited and insufficient in assessing aggregation propensity, including NNQQNY itself. Therefore, we first examined the aggregation of the NNQQNY peptide using TEM.

Our time-course TEM studies of NNQQNY suggest that no aggregation occurred during the first 2 weeks (data not shown), and only a few very long fibrillar aggregates (width = 8.69 ± 0.23 nm) were observed after 3 to 6 weeks (see Figure 2A), in agreement with our previous AFM study.[9] These observations are also consistent with the prediction of a low propensity for aggregation provided by PASTA and Zyggregator (see above). Previous works on CGNNQQNY in water (same solvent condition as ours) yielded aggregates in less than 1 week at a similar concentration (500−600 $\mu$M),[41] and GNNQQNY aggregated at time $t$ = 0 at higher concentrations (≈ 3.5 mM).[40] The discrepancy in aggregation propensity of the short and long versions of the Sup35 fragment suggests that the glycine residue plays a role or the overall peptide must reach a certain length (number of residues) to become aggregation-prone, as in the cases of polyglutamine and polyalanine.[13] In other words, a loss of glycine residue may shift the nucleation stage to a larger size oligomer. (GNNQQNY is predicted to nucleate at $n$ = 3 or 4.)[17,65] Such a shift appears to be consistent with the overall amino acid composition of the yeast prion family of proteins (Sup35p, Ure2p, and Rnq1p) that shares an enrichment in polar residues (N and Q).[12] Furthermore, a previous IM-MS study done by our group has shown that NNQQNY oligomers form isotropic oligomers through $n$ = 8 but start a nonisotropic pathway at $n$ = 9 containing $\beta$-sheet and are dominantly $\beta$-sheet at $n$ = 19 and 20 (see Figure 2B).[9] In this previous work, our group has also shown that only nonisotropic oligomers can seed nucleation and aggregation. Hence, the existence of these isotropic oligomers (up to $n$ = 16) and their abundance implies a long lag phase before aggregation.

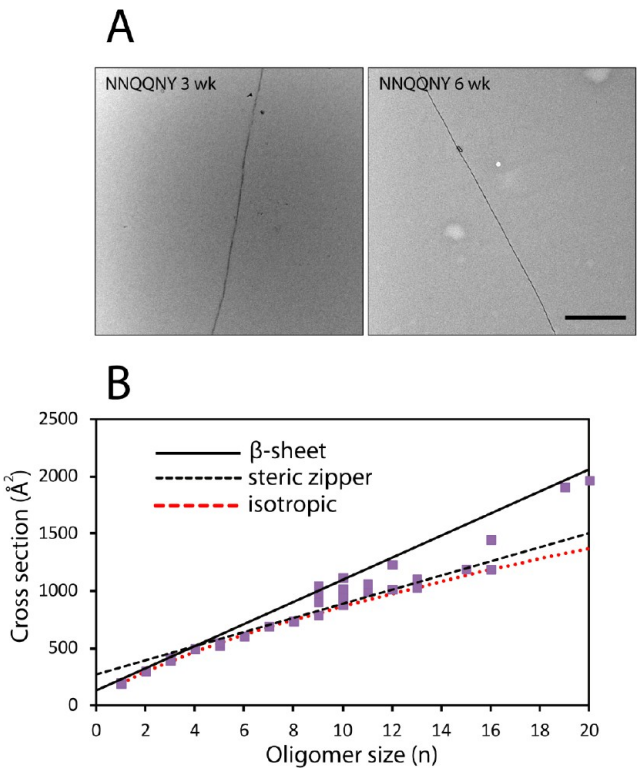


**Figure 2.** (A) Following extended incubation periods, TEM imaging of NNQQNY (400 $\mu$M) samples in water revealed occasional long fibers. The scale bar is 500 nm. (B) Experimental cross sections of NNQQNY as a function of time. The plot is reproduced from previous publication by Bleiholder et al. (ref 9) with the addition of theoretical steric zipper oligomer cross sections.

Computational simulations using advanced techniques such as replica-exchange MD theoretically sample the possible peptide conformations. However, the presence of abundant $\beta$-sheet conformations or pre-existing steric zipper structures observed by these methods at small oligomer sizes does not directly imply a high aggregation propensity because the internal rearrangement at large oligomer sizes may be very slow or kinetically inaccessible.[63] Some fibril-crystal distinctions in the packing of the peptide chains within the fiber and crystal forms of GNNQQNY have been shown by studies using diffraction analysis[40] and magic-angle-spinning NMR.[66] A recent elegant model proposed by Knowles and coworkers[67] has addressed the untwisting phenomenon of helical steric zipper during the transition from protofilaments to crystalline phase, which accounts for the discrepancies among the results obtained from measuring the protofilaments and the microcrystals. Nonetheless, the role of the steric zipper motif in self-assembly pathways, especially the kinetic aspect, remains unclear.

**IM-MS Suggests Replacing Polar Interactions with Hydrophobic Interactions, Which Increases The Self-Assembly Propensities of NNQQNY Mutants, Consistent with AFM and TEM Observations.** Figure 3 shows representative mass spectra of the six mutants. The peaks are labeled based on the oligomer size to charge ratios ($n/z$). Major peaks are $n/z$ 1/1, $n/z$ 3/2, and $n/z$ 5/3, and less abundant peaks locate at $n/z$ 4/3, $n/z$ 7/4, $n/z$ 9/5, $n/z$ 11/6, $n/z$ 12/7, $n/z$ 19/13, and so on. The mass spectra of NVVVVY (Figure 3A), NVVQIY (Figure 3C), and NVQVVY (Figure 3D) show intense signals for oligomer peaks, while the remaining three


dx.doi.org/10.1021/jp4046287 | J. Phys. Chem. B 2013, 117, 8436−8446

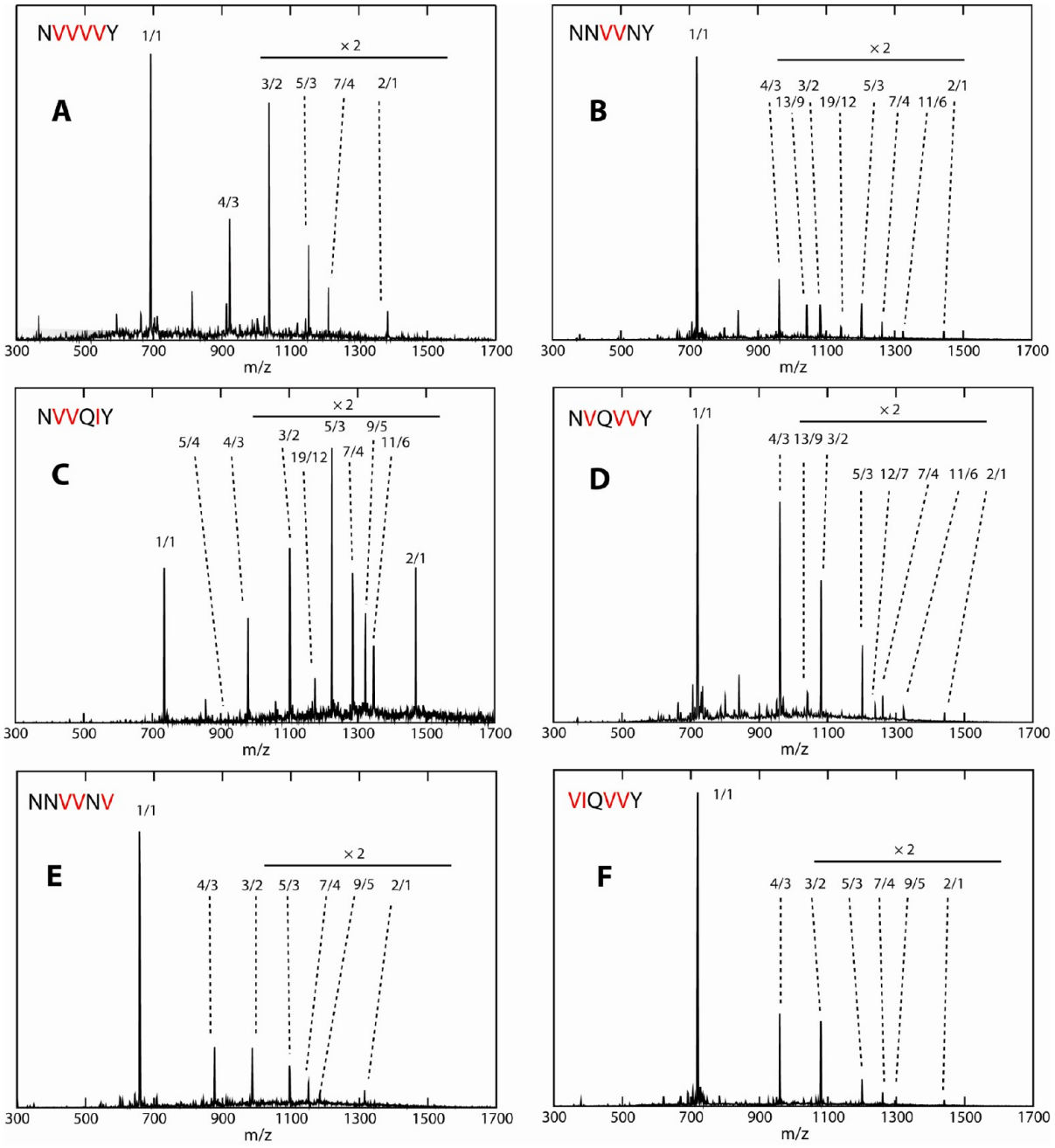


**Figure 3.** Peptide oligomerization and aggregation observed by IM-MS. The peptide concentration is 400 $\mu$M in water. ESI-quadrupole mass spectra show extensive oligomerization for all peptides. Peak annotations indicate $n/z$, where $n$ = number of oligomer and $z$ = charge.

NNVVNY (Figure 3B), NNVVNV (Figure 3E), and VIQVVY (Figure 3F) have lower signals for peaks at high $m/z$ values. The experimental cross sections are compared with three different models: the isotropic model, the steric zipper model, and the ideal $\beta$-sheet model. The two latter models are obtained from hypothetical zippers and $\beta$-sheets constructed from the X-ray crystal structure of NNQQNY using the RosettaProfile method. It is noted that the cross sections of ideal $\beta$-sheets are an upper bound rather than an exact structural comparison due to the tendency of structural dynamics to reduce the cross sections. A structural transition occurs at a specific oligomer number "$n$" or a "range of $n$", where the cross section significantly increases relative to smaller "$n$" and relative to the predictions of the isotropic progression line. The cross section analysis (see Figure 4) reveals extensive oligomerization for NNVVNY (Figure 4B), NVVQIY (Figure 4C), and NVQVVY(Figure 4D) and transitions from the isotropic to the $\beta$-sheet cross sections. Structures with cross sections in the range between steric zipper and $\beta$-sheet models are also observed at larger oligomer sizes. NVVVVY (Figure 4A) shows an early transition to nonisotropic oligomers at $n$ = 4, but oligomers larger than octamer are not found. Lastly, NNVVNV (Figure 4E) and VIQVVY (Figure 4F) show mainly isotropic cross sections, implying globular/amorphous aggregate formation only. Overall, the IM-MS data suggest that:

(1) NNVVNY, NVVQIY, and NVQVVY should aggregate to form fibrils.
(2) VIQVVY and NNVVNV should not form fibrillar aggregates.


dx.doi.org/10.1021/jp4046287 | J. Phys. Chem. B 2013, 117, 8436−8446

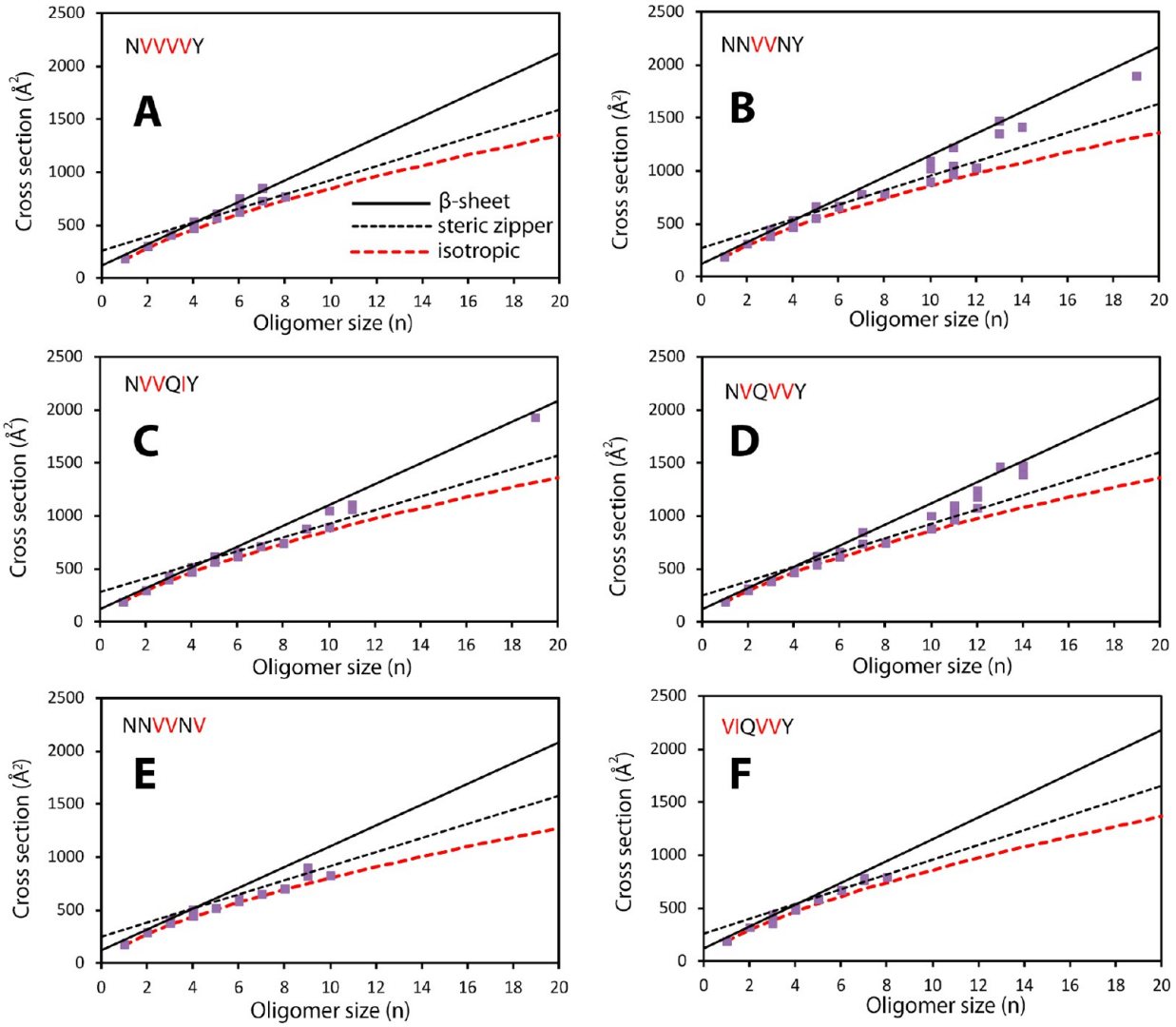


**Figure 4.** Experimental cross section (Å$^2$) as a function of oligomer size ($n$). (A) NVVVVY shows an early transition at $n$ = 4; $\beta$-sheet structures are observed from $n$ = 4 to 7. Structures with steric zipper cross sections are detected at $n$ = 6, 7, and 8. (B) NNVVNY shows transitions to steric zipper and $\beta$-sheet; isotropic cross sections are observed up to $n$ = 12 and primarily $\beta$-sheet structures for $n$ > 12. (C) NVVQIY shows a transition to $\beta$-sheet at $n$ = 10, and $\beta$-sheet structures are also at $n$ = 19; steric zipper formation also likely appears between $n$ = 4 and 11. (D) NVQVVY shows a transition from $n$ = 7 to 10, with $\beta$-sheet structures being observed up to $n$ = 14. (E) NNVVNV shows isotropic cross section up to $n$ = 10 with no $\beta$-sheet oligomers and only one steric zipper at $n$ = 9. (F) VIQVVY shows isotropic cross sections up to $n$ = 8 and no larger oligomers.

(3) NVVVVY aggregates quickly, evidenced by a very early transition from isotropic to $\beta$-sheet cross sections, although in our data the system is still in the transition zone at $n$ = 8, our largest observed oligomer.

Figure 5 (AFM) and Figure S2 in the Supporting Information (TEM) represent the microscopy data of the six mutants obtained after 3 to 4 week incubation periods. The four mutants containing Asn-1 and Tyr-6 (i.e., NVVVVY, NNVVNY, NVVQIY, and NVQVVY) aggregate extensively. Here we note that the fibril widths measured by AFM are often much larger than by electron microscopy due to convolution of surface features and the scanning tip.[68] Thus, the width values from AFM do not reflect the actual dimensions of the fibrils. Hence, the average fibril widths ($W$) are obtained from TEM images. We also report the average height ($H$) and length ($L$) for each of the fibrils from AFM images. The data are summarized in Table 2. NVVVVY fibrils (Figure 5A) have a well-defined morphology in which each chain grows separately and relatively long. NNVVNY (Figure 5B) shows clumps of short fibrils with poorly defined morphologies. NVVQIY (Figure 5C) populates short aggregates, which are consistently revealed by both AFM and TEM and are very low in height. The last mutant of the four, NVQVVY (Figure 5D), shows some regular fibers, similar to NVVVVY, and some aggregate inclusions (i.e., the late stage in the maturation of amorphous and fibrillar aggregates[69]), similar to those found in the NNVVNY.

The remaining two mutants form only isotropic oligomers, as shown by IM-MS. In AFM, NNVVNV shows some amorphous aggregates, whereas VIQVVY has very few short fibrils and mostly unstructured aggregates (Figure 5E,F). Very few fibril-like aggregates are captured by TEM, but their populations are very small compared with the other four peptides. We also report the widths of those aggregates in Table 2. Overall, the microscopy data are in excellent agreement with IM-MS observations in terms of aggregation propensities.

The above results suggest that within the steric zipper, valine residues provide hydrophobic interactions that can compensate


dx.doi.org/10.1021/jp4046287 | J. Phys. Chem. B 2013, 117, 8436−8446

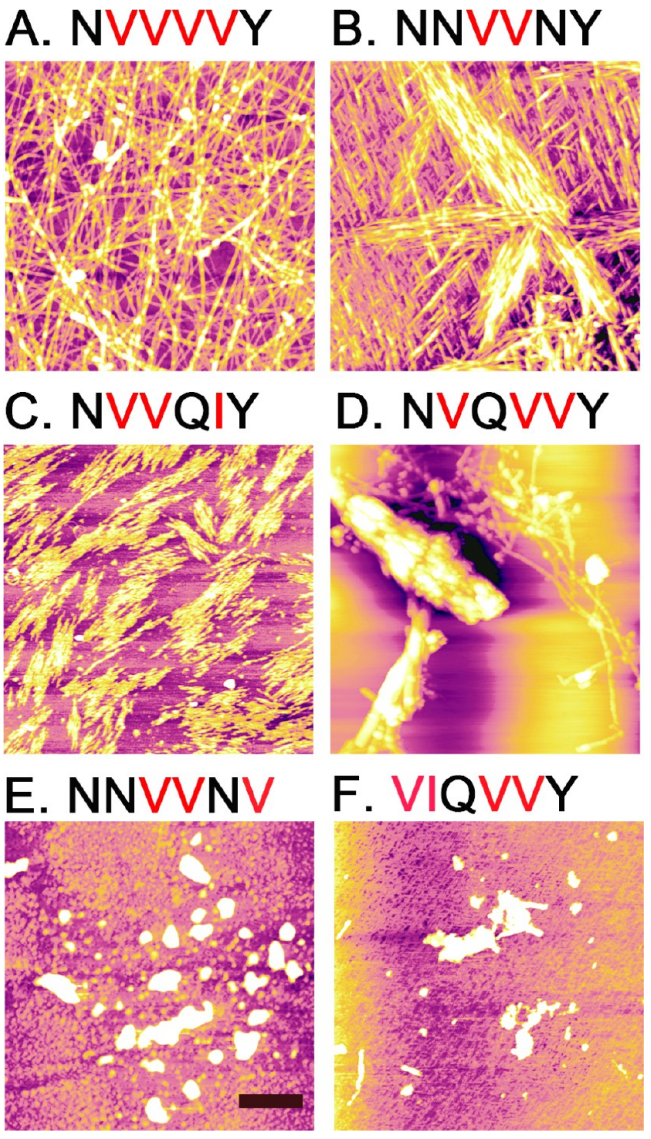


**Figure 5.** Representative AFM images of the six peptides. (A) NVVVVY shows abundant fibrillar aggregates. (B) NNVVNY forms packed short fibers. (C) NVVQIY shows packed, twisted, and short fibrils. (D) NVQVVY shows regular fibrils with some aggregate inclusions. (E) NNVVNV shows globular and amorphous aggregates. (F) VIQVVY shows unstructured aggregates with some short fibers. The scale bar is 1 $\mu$m.

**Table 2. Fibril Dimensions ($W$, $L$, and $H$ in nm) of the Six Peptide Mutants Obtained from AFM and TEM Measurements**

| peptides | width ($W$, nm) | length ($L$, nm) | height ($H$, nm) |
|---|---|---|---|
| NVVVVY | 7.77 ± 0.10 | 2739 ± 182 | 6.0 ± 0.6 |
| NNVVNY | 9.62 ± 0.14 | 874 ± 114 | 8.2 ± 0.6 |
| NVVQIY | 11.78 ± 0.34 | 538 ± 41 | 0.6 ± 0.03 |
| NVQVVY | 10.13 ± 0.18 | 846 ± 82 | 10 ± 0.5 |
| NNVVNV | 10.73 ± 0.38 | n/a | n/a |
| VIQVVY | 11.40 ± 0.25 | n/a | n/a |

for the loss of intrasheet hydrogen bonds between Gln-3 and Asn-5 and polar intersheet interactions (i.e., locking mechanism)[17] among opposite Gln-3 residues, as seen in the cases of NVVVVY, NNVVNY, and NVVQIY. The presence of isoleucine in the NVVQIY zipper enhances the hydrophobic character of the dry interface. The exposure of Gln-4 into the wet interface can be stabilized by hydrogen bonding with hydroxyl side chains of Tyr-6.[17] This hydrogen bonding interaction plays a crucial role because the replacement of Tyr-6 by Val-6 in NNVVNV destabilizes the zipper. Another factor contributing to the low aggregation propensity of this mutant is the loss of tyrosine $\pi$-stacking.

In NVQVVY, Gln-4 is replaced by less bulky Val-4, which has a better $\beta$-sheet propensity.[70] The locking mechanism formed by opposite Gln-3 residues in the steric zipper conformation[17] remains intact. However, as seen in MD simulations (discussed in the next section) and AFM images (Figure 5), the presence of Gln-3 does not provide this peptide with a better aggregation propensity compared with NVVVVY.

The mutant VIQVVY is the most interesting one. As previously mentioned, this mutant has attained high predicted scores, but our experiments do not show abundant formation of ordered fibrils. From the perspective of residue compositions, the substitution of Ile-2 for Asn-2 leads to the exposure of a very hydrophobic residue on the solvent side of the steric zipper. Although many peptides containing hydrophobic pairs (e.g., II, IV, IL) have been reported to aggregate, in many cases the aggregation can only be initiated by anionic cofactors such as heparin,[31,71] or their propensities can be strongly dependent on experimental conditions (pH, ionic strength) and protein concentrations.[72,73] Therefore, VIQVVY in water may have much slower aggregation kinetics than the other mutants (except NNVVNV) or it may undergo some nucleation forms other than steric zipper to form amorphous aggregates and short fibrils.

**Evidence That Steric Zipper Stability Enhances Aggregation Propensity and Controls Fibrillar Morphology.** The purpose of the MD simulations here is not to sample new structures but to briefly examine the stability of steric zipper decamers. The initial conformations are shown in Figure S3 in the Supporting Information. The final structures obtained from the MD simulations starting with steric zipper conformations are shown in Figure S4 in the Supporting Information. The simulation-derived structures are characterized based on the distribution of average center-of-mass distances between $\beta$-sheet layers (Figure 6A). NVVVVY, NNVVNV, VIQVVY, and NVVQIY have a single population centered at 1.00 to 1.25 nm, the typical distance between adjacent layers in steric zipper conformations. From these data, it is clear that the steric zipper decamers of NVVVVY and NVVQIY are stable after 100 ns simulations with a minimal change in RMSD (see Figure S5 in the Supporting Information) and distances between layers. These decamer structures are also stabilized by 50−60 hydrogen bonds on average (Figure 6B). The other two steric zipper decamers with a unimodal distribution are less stable, evidenced by a large fluctuation in RMSD, a wider distribution (NNVVNV), or larger distances than expected (VIQVVY). VIQVVY also has a fewer hydrogen bonds compared with the other peptides.

NNVVNY and NVQVVY exhibit a bimodal distribution between $\beta$-sheet layers with two populations centered near 1.00 to 1.25 nm and 1.50 to 2.50 nm (Figure 6A). These $\beta$-sheet distances represent the transition from bilayer to trilayer steric zippers. The dimensions of $\beta$-fibrils for these peptides are similar in size, ~10 nm in width (see Table 2) and independent of peptide length.[20] Oligomers with two different steric zipper interfaces (e.g., NKGAII)[18] have also been observed by X-ray crystallography. Our AFM images of the fibrils observed for


dx.doi.org/10.1021/jp4046287 | J. Phys. Chem. B 2013, 117, 8436−8446

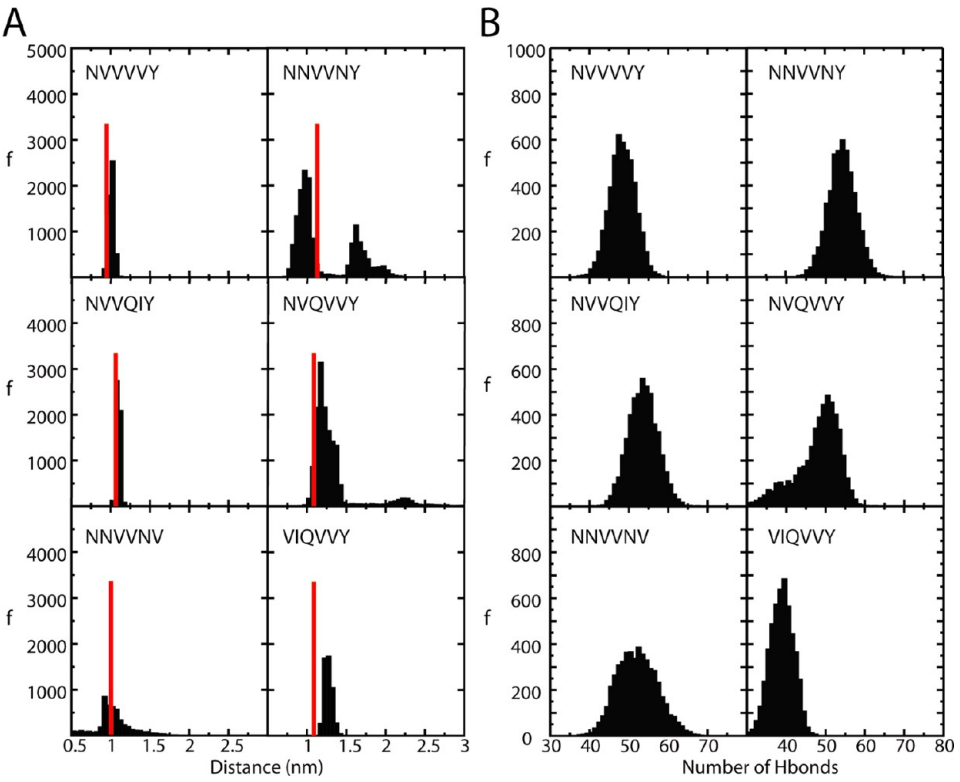


**Figure 6.** (A) Distributions of average distances between $\beta$-sheet layers obtained by MD simulations. The red line indicates the distance between the two $\beta$-sheets of the zipper predicted by the RosettaProfile model. (B) Hydrogen-bond distributions obtained from MD simulation starting with steric zipper conformations.

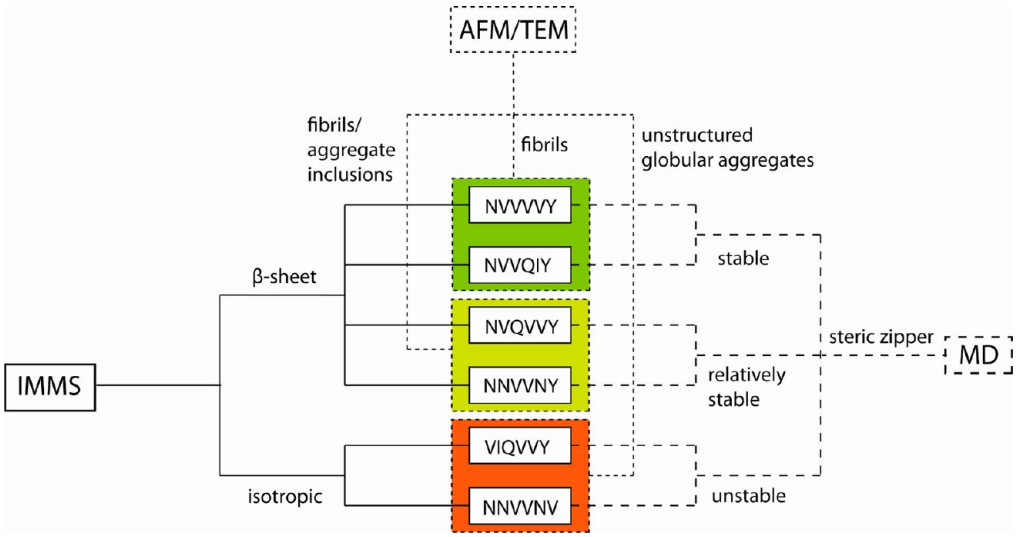


**Figure 7.** Summary of experimental and computational results obtained from IM-MS, AFM/TEM, and MD simulations. The overall data indicate that the stability of steric zipper increases aggregation propensity and controls fibril morphology.

these two peptides show the presence of aggregation inclusions. (See Figure 5.) These observations together with the MD simulations suggest that the aggregation process of the two peptides NNVVNY and NVQVVY may follow a pathway in which multiple-layer steric zippers assist the formation of fibrils and aggregate inclusions.

Overall, we observe stable steric zipper decamers for the four peptides NVVVVY, NNVVNY, NVVQIY, and NVQVVY after 100 ns simulations. This observation correlates well with experimental data, showing that these four peptides are aggregation-prone. We conclude that accessibility to stable steric zipper conformations facilitates the nucleation and fibril formation for these peptides.

Figure 7 summarizes the experimental and computational data obtained for the six peptides. In general, there is a good agreement among the three different techniques (IM-MS, MD, and microscopy). The peptides with $\beta$-sheet oligomers probed by IM-MS form fibrils observed by AFM/TEM. This is partially explained by MD simulations that show steric zipper


dx.doi.org/10.1021/jp4046287 | J. Phys. Chem. B 2013, 117, 8436−8446

stabilization facilitates peptide aggregation and disruption of the steric zipper motif inhibits fibril formation.

**Aggregation Propensities of the Mutants in Water Are in Moderate Agreement with Theoretical Predictions.** According to our experimental data, the four most aggregating peptides are NVVVVY, NVVQIY, NVQVVY, and NNVVNY, whereas the other two peptides VIQVVY and NNVVNV do not form fibrils in water. As mentioned above, VIQVVY is an unexpectedly interesting case because predictions and experiments show opposite results. The PASTA method predicted 3/6 peptides correctly (i.e., NVVVVY, NVQVVY, and NVVQIY in the top 4). The RosettaProfile method (i.e., steric zipper method) ties with PASTA for 3/6 peptides in the top 4 (i.e., NVVQIY, NVQVVY, and NVVVVY; see Table 1). The Zyggregator method is the best of all with 4/6.

Although PASTA and RosettaProfile have similar success rates as shown above, their procedures for obtaining the scores are rather different. PASTA mainly considers interactions within single $\beta$-sheet layers in either antiparallel or parallel configurations. In general, residues with high hydrophobicity values and $\beta$-sheet propensity such as valine or isoleucine provide positive effects toward high aggregation propensity, while opposite effects are expected for hydrophilic residues such as asparagine.[36,37] As a result, PASTA scores are proportional to hydrophobicity. This method ranks both VIQVVY and NNVVNV on the top of the list, which contradicts experimental results. RosettaProfile correctly predicts NNVVNV as a weak aggregator. However, RosettaProfile may be biased by the polar interactions provided by Gln and Asn residues, as NNQQNY is not the best-suited model for hydrophobic systems. Therefore, RosettaProfile can improve its success rate for hydrophobic sequences by using a more hydrophobic model such as VEALYL[9] and GGVVIA.[8] Eisenberg and coworkers have shown that hydrophobic sequences such as VEALYL and GGVVIA can form different classes of steric zipper than that of NNQQNY.[18]

Zyggregator turns out to be the best method. The only disagreement between the experimental observations and the predictions is VIQVVY. Zyggregator gives a low score to NNVVNV (1.18; below 1.20 is weakly aggregating) and ranks the four aggregating sequence as NVVVVY $\gg$ NVQVVY $\approx$ NVVQIY $\approx$ NNVVNY.

## SUMMARY AND CONCLUSIONS

The aggregation processes of the six Sup35 mutants (NVVVVY, NNVVNY, NVVQIY, NVQVVY, NNVVNV, and VIQVVY) have been studied by a combination of techniques including IM-MS, AFM, TEM, and MD simulations. From the progression of cross sections as a function of oligomer sizes, IM-MS shows isotropic oligomers formed almost exclusively for NNVVNV and VIQVVY, whereas $\beta$-sheet oligomers are preferred for the other four. This result is consistent with observations by AFM and TEM, showing the presences of fibrillar oligomers in the cases of NVVVVY, NNVVNY, NVVQIY, and NVQVVY. We have shown that mutations that remove polar interactions from the dry interface of the steric zipper structure can increase aggregation propensities.

Our MD simulations show that the relative stability of steric zipper conformations is in good agreement with the aggregation propensity of the peptide. The stabilizing factor at the zipper interface is not specific to Asn and Gln residues, as evidenced by the high stability of steric zipper decamers of NVVVVY and NVVQIY during 100 ns explicit solvent MD simulations. The other two aggregating peptides, NNVVNY and NVQVVY, also have stable structures and a tendency to form multiple-layer steric zippers, as shown by the presence of aggregation inclusions in the AFM images.

## ASSOCIATED CONTENT

### Supporting Information

TEM images of the six peptide mutants, detailed experimental procedure for IM-MS, representative ATDs, and additional Figures. This material is available free of charge via the Internet at http://pubs.acs.org.

## AUTHOR INFORMATION

### Corresponding Author

*E-mail: bowers@chem.ucsb.edu. Tel: +1-805-893-2673.

### Notes

The authors declare no competing financial interest.

## ACKNOWLEDGMENTS

This research was funded by the National Science Foundation under grant CHE-0909743 (M.T.B.). We thank Ms. Margaret Condron for synthesizing the peptides. We acknowledge the use of the NRI-MCDB Microscopy Facility at UC, Santa Barbara. T.D.D. thanks Erin Brocker for useful comments and proof reading. N.J.E. acknowledges the National Science Foundation for a Graduate Student Research Fellowship. Support from the MURI and DURIP programs of the U.S. Army Research Laboratory and U.S. Army Research Office under grant nos. DAAD 19-03-1-0121 and W911NF-09-1-0280 for purchase of the AFM instrument is gratefully acknowledged (S.K.B.). This research was also partially supported by the National Science Foundation through TeraGrid resources provided by the Texas Advanced Computing Center under grant number TG-CHE130004 (M.T.B.).

## REFERENCES

(1) Eisenberg, D.; Nelson, R.; Sawaya, M. R.; Balbirnie, M.; Madsen, A.; Riekel, C.; Sambashivan, S.; Liu, Y.; Gingery, M.; Grothe, R. Structural Studies of Amyloid. *FEBS J.* **2005**, *272*, 78−79.

(2) Laganowsky, A.; Liu, C.; Sawaya, M. R.; Whitelegge, J. P.; Park, J.; Zhao, M. L.; Pensalfini, A.; Soriaga, A. B.; Landau, M.; Teng, P. K.; Cascio, D.; Glabe, C.; Eisenberg, D. Atomic View of a Toxic Amyloid Small Oligomer. *Science* **2012**, *335*, 1228−1231.

(3) Chiti, F.; Dobson, C. M. Amyloid Formation by Globular Proteins under Native Conditions. *Nat. Chem. Biol.* **2008**, *5*, 15−21.

(4) Klein, W. L.; Krafft, G. A.; Finch, C. E. Targeting Small a $\beta$ Oligomers: The Solution to an Alzheimer's Disease Conundrum? *Trends Neurosci.* **2001**, *24*, 219−224.

(5) McKhann, G.; Drachman, D.; Folstein, M.; Katzman, R.; Price, D.; Stadlan, E. M. Clinical Diagnosis of Alzheimer's Disease: Report of the Nincds-Adrda Work Group under the Auspices of Department of Health and Human Services Task Force on Alzheimer's Disease. *Neurology* **1984**, *34*, 939−944.

(6) Haass, C.; Selkoe, D. J. Soluble Protein Oligomers in Neurodegeneration: Lessons from the Alzheimer's Amyloid $\beta$-Peptide. *Nat. Rev. Mol. Cell Biol.* **2007**, *8*, 101−112.

(7) Fernandez-Escamilla, A. M.; Rousseau, F.; Schymkowitz, J.; Serrano, L. Prediction of Sequence-Dependent and Mutational Effects on the Aggregation of Peptides and Proteins. *Nat. Biotechnol.* **2004**, *22*, 1302−1306.

(8) Sawaya, M. R.; Sambashivan, S.; Nelson, R.; Ivanova, M. I.; Sievers, S. A.; Apostol, M. I.; Thompson, M. J.; Balbirnie, M.; Wiltzius, J. J. W.; McFarlane, H. T.; Madsen, A. O.; Riekel, C.; Eisenberg, D.

Atomic Structures of Amyloid Cross-$\beta$ Spines Reveal Varied Steric Zippers. *Nature* **2007**, *447*, 453−457.
(9) Bleiholder, C.; Dupuis, N. F.; Wyttenbach, T.; Bowers, M. T. Ion Mobility-Mass Spectrometry Reveals a Conformational Conversion from Random Assembly to $\beta$-Sheet in Amyloid Fibril Formation. *Nat. Chem.* **2011**, *3*, 172−177.
(10) Conway, K. A.; Lee, S. J.; Rochet, J. C.; Ding, T. T.; Williamson, R. E.; Lansbury, P. T. Acceleration of Oligomerization, Not Fibrillization, Is a Shared Property of Both $\alpha$-Synuclein Mutations Linked to Early-Onset Parkinson's Disease: Implications for Pathogenesis and Therapy. *Proc. Natl. Acad. Sci. U.S.A.* **2000**, *97*, 571−576.
(11) Caflisch, A. Computational Models for the Prediction of Polypeptide Aggregation Propensity. *Curr. Opin. Chem. Biol.* **2006**, *10*, 437−444.
(12) Kabani, M.; Melki, R. Yeast Prions Assembly and Propagation Contributions of the Prion and Non-Prion Moieties and the Nature of Assemblies. *Prion* **2011**, *5*, 277−284.
(13) Bernacki, J. P.; Murphy, R. M. Length-Dependent Aggregation of Uninterrupted Polyalanine Peptides. *Biochemistry* **2011**, *50*, 9200−9211.
(14) Wiltzius, J. J. W.; Sievers, S. A.; Sawaya, M. R.; Cascio, D.; Popov, D.; Riekel, C.; Eisenberg, D. Atomic Structure of the Cross-$\beta$ Spine of Islet Amyloid Polypeptide (Amylin). *Protein Sci.* **2008**, *17*, 1467−1474.
(15) Tsemekhman, K.; Goldschmidt, L.; Eisenberg, D.; Baker, D. Cooperative Hydrogen Bonding in Amyloid Formation. *Protein Sci.* **2007**, *16*, 761−764.
(16) Balbirnie, M.; Grothe, R.; Eisenberg, D. S. An Amyloid-Forming Peptide from the Yeast Prion Sup35 Reveals a Dehydrated Beta-Sheet Structure for Amyloid. *Proc. Natl. Acad. Sci. U.S.A.* **2001**, *98*, 2375−2380.
(17) Nelson, R.; Sawaya, M. R.; Balbirnie, M.; Madsen, A. O.; Riekel, C.; Grothe, R.; Eisenberg, D. Structure of the Cross-Beta Spine of Amyloid-Like Fibrils. *Nature* **2005**, *435*, 773−778.
(18) Colletier, J.-P.; Laganowsky, A.; Landau, M.; Zhao, M.; Soriaga, A. B.; Goldschmidt, L.; Flot, D.; Cascio, D.; Sawaya, M. R.; Eisenberg, D. Molecular Basis for Amyloid-$\beta$ Polymorphism. *Proc. Natl. Acad. Sci. U.S.A.* **2011**, 16938−16943.
(19) Uversky, V. N. Mysterious Oligomerization of the Amyloidogenic Proteins. *FEBS J.* **2010**, *277*, 2940−2953.
(20) Ivanova, M. I.; Sawaya, M. R.; Gingery, M.; Attinger, A.; Eisenberg, D. An Amyloid-Forming Segment of $\beta$ 2-Microglobulin Suggests a Molecular Model for the Fibril. *Proc. Natl. Acad. Sci. U.S.A.* **2004**, *101*, 10584−10589.
(21) Sipe, J. D.; Cohen, A. S. Review: History of the Amyloid Fibril. *J. Struct. Biol.* **2000**, *130*, 88−98.
(22) Ivanova, M. I.; Thompson, M. J.; Eisenberg, D. A Systematic Screen of $\beta$(2)-Microglobulin and Insulin for Amyloid-Like Segments. *Proc. Natl. Acad. Sci. U.S.A.* **2006**, *103*, 4079−4082.
(23) Nelson, R.; Eisenberg, D. Recent Atomic Models of Amyloid Fibril Structure. *Curr. Opin. Struc. Biol.* **2006**, *16*, 260−265.
(24) Thompson, M. J.; Sievers, S. A.; Karanicolas, J.; Ivanova, M. I.; Baker, D.; Eisenberg, D. The 3D Profile Method for Identifying Fibril-Forming Segments of Proteins. *Proc. Natl. Acad. Sci. U.S.A.* **2006**, *103*, 4074−4078.
(25) Goldschmidt, L.; Teng, P. K.; Riek, R.; Eisenberg, D. Identifying the Amylome, Proteins Capable of Forming Amyloid-Like Fibrils. *Proc. Natl. Acad. Sci. U.S.A.* **2010**, *107*, 3487−3492.
(26) Moore, C. L.; Huang, M. H.; Robbennolt, S. A.; Voss, K. R.; Combs, B.; Gamblin, T. C.; Goux, W. J. Secondary Nucleating Sequences Affect Kinetics and Thermodynamics of Tau Aggregation. *Biochemistry* **2011**, *50*, 10876−10886.
(27) Matthes, D.; Gapsys, V.; Daebel, V.; de Groot, B. L. Mapping the Conformational Dynamics and Pathways of Spontaneous Steric Zipper Peptide Oligomerization. *PLoS One* **2011**, *6*, e19129.
(28) Stanzione, F.; De Simone, A.; Esposito, L.; Vitagliano, L. Dynamical Properties of Steric Zipper Polymorphs Formed by a IAPP-Derived Peptide. *Protein Pept. Lett.* **2012**, *19*, 846−851.
(29) Park, J.; Kahng, B.; Hwang, W. Thermodynamic Selection of Steric Zipper Patterns in the Amyloid Cross-$\beta$ Spine. *PLoS Comput. Biol.* **2009**, *5*, e1000492.
(30) Matthes, D.; Gapsys, V.; de Groot, B. L. Driving Forces and Structural Determinants of Steric Zipper Peptide Oligomer Formation Elucidated by Atomistic Simulations. *J. Mol. Biol.* **2012**, *421*, 390−416.
(31) Daebel, V.; Chinnathambi, S.; Biernat, J.; Schwalbe, M.; Habenstein, B.; Loquet, A.; Akoury, E.; Tepper, K.; Muller, H.; Baldus, M.; Griesinger, C.; Zweckstetter, M.; Mandelkow, E.; Vijayan, V.; Lange, A. $\beta$-Sheet Core of Tau Paired Helical Filaments Revealed by Solid-State NMR. *J. Am. Chem. Soc.* **2012**, *134*, 13982−13989.
(32) Lee, S. W.; Mou, Y.; Lin, S. Y.; Chou, F. C.; Tseng, W. H.; Chen, C. H.; Lu, C. Y.; Yu, S. S.; Chan, J. C. Steric Zipper of the Amyloid Fibrils Formed by Residues 109−122 of the Syrian Hamster Prion Protein. *J. Mol. Biol.* **2008**, *378*, 1142−1154.
(33) Berhanu, W. M.; Masunov, A. E. Unique Example of Amyloid Aggregates Stabilized by Main Chain H-Bond Instead of the Steric Zipper: Molecular Dynamics Study of the Amyloidogenic Segment of Amylin Wild-Type and Mutants. *J. Mol. Model.* **2012**, *18*, 891−903.
(34) Berryman, J. T.; Radford, S. E.; Harris, S. A. Thermodynamic Description of Polymorphism in Q- and N-Rich Peptide Aggregates Revealed by Atomistic Simulation. *Biophys. J.* **2009**, *97*, 1−11.
(35) Zheng, J.; Ma, B.; Tsai, C. J.; Nussinov, R. Structural Stability and Dynamics of an Amyloid-Forming Peptide GNNQQNY from the Yeast Prion Sup-35. *Biophys. J.* **2006**, *91*, 824−833.
(36) Trovato, A.; Chiti, F.; Maritan, A.; Seno, F. Insight into the Structure of Amyloid Fibrils from the Analysis of Globular Proteins. *Plos Comput. Biol.* **2006**, *2*, 1608−1618.
(37) Trovato, A.; Seno, F.; Tosatto, S. C. E. The Pasta Server for Protein Aggregation Prediction. *Protein Eng., Des. Sel.* **2007**, *20*, 521−523.
(38) Pawar, A. P.; Dubay, K. F.; Zurdo, J.; Chiti, F.; Vendruscolo, M.; Dobson, C. M. Prediction of "Aggregation-Prone" and "Aggregation-Susceptible" Regions in Proteins Associated with Neurodegenerative Diseases. *J. Mol. Biol.* **2005**, *350*, 379−392.
(39) Tartaglia, G. G.; Pawar, A. P.; Campioni, S.; Dobson, C. M.; Chiti, F.; Vendruscolo, M. Prediction of Aggregation-Prone Regions in Structured Proteins. *J. Mol. Biol.* **2008**, *380*, 425−436.
(40) Marshall, K. E.; Hicks, M. R.; Williams, T. L.; Hoffmann, S. V.; Rodger, A.; Dafforn, T. R.; Serpell, L. C. Characterizing the Assembly of the Sup35 Yeast Prion Fragment, GNNQQNY: Structural Changes Accompany a Fiber-to-Crystal Switch. *Biophys. J.* **2010**, *98*, 330−338.
(41) Portillo, A. M.; Krasnoslobodtsev, A. V.; Lyubchenko, Y. L. Effect of Electrostatics on Aggregation of Prion Protein Sup35 Peptide. *J. Phys.: Condens. Mat.* **2012**, 24.
(42) Wyttenbach, T.; Bowers, M. T. Structural Stability from Solution to the Gas Phase: Native Solution Structure of Ubiquitin Survives Analysis in a Solvent-Free Ion Mobility-Mass Spectrometry Environment. *J. Phys. Chem. B* **2011**, *115*, 12266−12275.
(43) Bernstein, S. L.; Dupuis, N. F.; Lazo, N. D.; Wyttenbach, T.; Condron, M. M.; Bitan, G.; Teplow, D. B.; Shea, J.-E.; Ruotolo, B. T.; Robinson, C. V.; Bowers, M. T. Amyloid-$\beta$ Protein Oligomerization and the Importance of Tetramers and Dodecamers in the Aetiology of Alzheimer's Disease. *Nat. Chem.* **2009**, *1*, 326−331.
(44) Kemper, P. R.; Dupuis, N. F.; Bowers, M. T.; New, A. Higher Resolution, Ion Mobility Mass Spectrometer. *Int. J. Mass. Spectrom.* **2009**, *287*, 46−57.
(45) Mason, E. A. *Transport Properties of Ions in Gases*, 99th ed.; John Wiley & Sons: New York, 1988.
(46) Gidden, J.; Ferzoco, A.; Baker, E. S.; Bowers, M. T. Duplex Formation and the Onset of Helicity in Poly D$(CG)_n$ Oligonucleotides in a Solvent-Free Environment. *J. Am. Chem. Soc.* **2004**, *126*, 15132−15140.
(47) Bushnell, J. E.; Kemper, P. R.; Bazan, G. C.; Bowers, M. T. The Determination of Cis-Trans Conformations in Tetrahedral *p*-Phenylene Vinylene Oligomers. *J. Phys. Chem. A* **2004**, *108*, 7730−7735.
(48) Hess, B.; Kutzner, C.; Spoel, D. v. d.; Lindahl, E. Gromacs 4: Algorithms for Highly Efficient, Load-Balanced, and Scalable Molecular Simulation. *J. Chem. Theory Comput.* **2008**, *4*, 435−437.

(49) Spoel, D. V. D.; Lindahl, E.; Hess, B.; Groenhof, G.; Mark, A. E.; Berendsen, H. J. C. Gromacs: Fast, Flexible, and Free. *J. Comput. Chem.* **2005**, *26*, 1701−1718.
(50) Damm, W.; Halgren, T. A.; Murphy, R. B.; Smondyrev, A. M.; Friesner, R. A.; Jorgensen, W. L. Opls_2002: A New Version of the OPLS-AA Force Field. *Abstr. Pap. Am. Chem. Soc.* **2002**, *224*, U471−U471.
(51) Halgren, T. A.; Murphy, R. B.; Jorgensen, W. L.; Friesner, R. A. Extending the OPLS-AA Force Field for Ligand Functionality. *Abstr. Pap. Am. Chem. Soc.* **2000**, *220*, U277−U277.
(52) Jorgensen, W. L.; Maxwell, D. S.; TiradoRives, J. Development and Testing of the OPLS All-Atom Force Field on Conformational Energetics and Properties of Organic Liquids. *J. Am. Chem. Soc.* **1996**, *118*, 11225−11236.
(53) Jorgensen, W. L.; Chandrasekhar, J.; Madura, J. D.; Impey, R. W.; Klein, M. L. Comparison of Simple Potential Functions for Simulating Liquid Water. *J. Chem. Phys.* **1983**, *79*, 926−935.
(54) Hess, B.; Bekker, H.; Berendsen, H. J. C.; Fraaije, J. G. E. M. Lincs: A Linear Constraint Solver for Molecular Simulations. *J. Comput. Chem.* **1997**, *18*, 1463−1472.
(55) Miyamoto, S.; Kollman, P. A. Settle - an Analytical Version of the Shake and Rattle Algorithm for Rigid Water Models. *J. Comput. Chem.* **1992**, *13*, 952−962.
(56) Darden, T.; York, D.; Pedersen, L. Particle Mesh Ewald: An N·Log(N) Method for Ewald Sums in Large Systems. *J. Chem. Phys.* **1993**, *98*, 10089−10093.
(57) Essmann, U.; Perera, L.; Berkowitz, M. L.; Darden, T.; Lee, H.; Pedersen, L. G.; Smooth, A. Particle Mesh Ewald Method. *J. Chem. Phys.* **1995**, *103*, 8577−8593.
(58) Evans, D. J.; Holian, B. L. The Nose-Hoover Thermostat. *J. Chem. Phys.* **1985**, *83*, 4069−4074.
(59) Periole, X.; Rampioni, A.; Vendruscolo, M.; Mark, A. E. Factors That Affect the Degree of Twist in $\beta$-Sheet Structures: A Molecular Dynamics Simulation Study of a Cross-Beta Filament of the GNNQQNY Peptide. *J. Phys. Chem. B* **2009**, *113*, 1728−1737.
(60) Lipfert, J.; Franklin, J.; Wu, F.; Doniach, S. Protein Misfolding and Amyloid Formation for the Peptide GNNQQNY from Yeast Prion Protein Sup35: Simulation by Reaction Path Annealing. *J. Mol. Biol.* **2005**, *349*, 648−658.
(61) Vitagliano, L.; Esposito, L.; Pedone, C.; De Simone, A. Stability of Single Sheet GNNQQNY Aggregates Analyzed by Replica Exchange Molecular Dynamics: Antiparallel Versus Parallel Association. *Biochem. Biophys. Res. Commun.* **2008**, *377*, 1036−1041.
(62) De Simone, A.; Esposito, L.; Pedone, C.; Vitagliano, L. Insights into Stability and Toxicity of Amyloid-Like Oligomers by Replica Exchange Molecular Dynamics Analyses. *Biophys. J.* **2008**, *95*, 1965−1973.
(63) Strodel, B.; Whittleston, C. S.; Wales, D. J. Thermodynamics and Kinetics of Aggregation for the GNNQQNY Peptide. *J. Am. Chem. Soc.* **2007**, *129*, 16005−16014.
(64) Reddy, A. S.; Chopra, M.; de Pablo, J. J. GNNQQNY-Investigation of Early Steps During Amyloid Formation. *Biophys. J.* **2010**, *98*, 1038−1045.
(65) Qi, X. H.; Hong, L.; Zhang, Y. A Variational Model for Oligomer-Formation Process of GNNQQNY Peptide from Yeast Prion Protein Sup35. *Biophys. J.* **2012**, *102*, 597−605.
(66) Lewandowski, J. R.; van der Wel, P. C. A.; Rigney, M.; Grigorieff, N.; Griffin, R. G. Structural Complexity of a Composite Amyloid Fibril. *J. Am. Chem. Soc.* **2011**, *133*, 14686−14698.
(67) Knowles, T. P. J.; De Simone, A.; Fitzpatrick, A. W.; Baldwin, A.; Meehan, S.; Rajah, L.; Vendruscolo, M.; Welland, M. E.; Dobson, C. M.; Terentjev, E. M., Twisting Transition between Crystalline and Fibrillar Phases of Aggregated Peptides. *Phys. Rev. Lett.* **2012**, *109*.
(68) Chamberlain, A. K.; MacPhee, C. E.; Zurdo, J.; Morozova-Roche, L. A.; Hill, H. A. O.; Dobson, C. M.; Davis, J. J. Ultrastructural Organization of Amyloid Fibrils by Atomic Force Microscopy. *Biophys. J.* **2000**, *79*, 3282−3293.
(69) Burke, K. A.; Godbey, J.; Legleiter, J. Assessing Mutant Huntingtin Fragment and Polyglutamine Aggregation by Atomic Force Microscopy. *Methods* **2011**, *53*, 275−284.
(70) Bellesia, G.; Jewett, A. I.; Shea, J. E. Sequence Periodicity and Secondary Structure Propensity in Model Proteins. *Protein Sci.* **2010**, *19*, 141−154.
(71) Larini, L.; Gessel, M. M.; Lapointe, N. E.; Do, T. D.; Bowers, M. T.; Feinstein, S. C.; Shea, J. E. Initiation of Assembly of Tau(273−284) and Its ΔK280 Mutant: An Experimental and Computational Study. *Phys. Chem. Chem. Phys.* **2013**, *15*, 8916−8928.
(72) de la Paz, M. L.; Goldie, K.; Zurdo, J.; Lacroix, E.; Dobson, C. M.; Hoenger, A.; Serrano, L. De Novo Designed Peptide-Based Amyloid Fibrils. *Proc. Natl. Acad. Sci. U.S.A.* **2002**, *99*, 16052−16057.
(73) Yoshimura, Y.; Lin, Y. X.; Yagi, H.; Lee, Y. H.; Kitayama, H.; Sakurai, K.; So, M.; Ogi, H.; Naiki, H.; Goto, Y. Distinguishing Crystal-Like Amyloid Fibrils and Glass-Like Amorphous Aggregates from Their Kinetics of Formation. *Proc. Natl. Acad. Sci. U.S.A.* **2012**, *109*, 14446−14451.